

Supplementary Materials for

Human cohesin compacts DNA by loop extrusion

Yoori Kim*, Zhubing Shi*, Hongshan Zhang, Ilya J. Finkelstein†, Hongtao Yu†

*These authors contributed equally to this work.

†Corresponding author. Email: ilya@finkelsteinlab.org (I.J.F.); hongtao.yu@utsouthwestern.edu (H.Y.).

Published 28 November 2019 on *Science* First Release

DOI: [10.1126/science.aaz4475](https://doi.org/10.1126/science.aaz4475)

This PDF file includes:

Materials and Methods

Figs. S1 to S8

Captions for Movies S1 to S9

References

Other Supplementary Material for this manuscript includes the following:

(available at science.scienmag.org/cgi/content/full/science.aaz4475/DC1)

Movies S1 to S9

Materials and Methods

Protein expression and purification

Human SMC1A and SMC3 genes were cloned into the pLIB vector separately and then combined into the pBIG1a vector by Gibson assembly (36). Sequences encoding human RAD21, STAG1, and the C-terminal region of NIPBL (NIPBL^C ; residues 1163-2804) were codon-optimized for insect cell expression (Integrated DNA Technologies). RAD21 was cloned into a modified pFastBac vector (Thermo Fisher) with a C-terminal TEV cleavage site followed by an MBP tag. STAG1 was cloned into a modified pFastBac vector with a C-terminal 3C protease cleavage site followed by a Twin-StrepII and His dual tag. NIPBL^C was cloned into a modified pFastBac with an N-terminal His and MBP dual tag followed by a 3C protease cleavage site. Baculoviruses were generated using the Bac-to-BacTM Baculovirus Expression System (Thermo Fisher). SMC1A, SMC3, and RAD21, with or without NIPBL^C , were co-expressed in High Five cells (Thermo Fisher), while STAG1 was expressed separately. Typically, a total of 40 ml P2 or P3 viruses were used to infect 800 ml High Five cells. High Five cells were harvested 48 h post infection.

High Five cells expressing STAG1 were resuspended in the Lysis Buffer HK500 (20 mM HEPES pH 7.5, 500 mM KCl, 10% glycerol, 5 mM 2-mercaptoethanol, 20 mM imidazole) plus 1 × PierceTM EDTA-free Protease Inhibitor Tablets (Thermo Fisher), 25 U ml⁻¹ PierceTM Universal Nuclease for Cell Lysis (Thermo Fisher), and 1 mM PMSF. Cells were lysed by a high-pressure homogenizer (Microfluidics LM-20), and cleared by centrifugation at 40,000 g for 1.5 h at 4°C. The supernatant was mixed with 2 ml Ni²⁺-NTA Agarose (Qiagen) for 1 h at 4°C. The resin was washed with Lysis Buffer HK500 followed by Lysis Buffer HK150 (20 mM HEPES pH 7.5, 150 mM KCl, 10% glycerol, 5 mM 2-mercaptoethanol, 2 mM MgCl₂, 0.01% Tween-20) plus 20 mM imidazole, and eluted by the Lysis Buffer HK150 plus 300 mM imidazole. The C-terminal Twin-StrepII and His dual tag in STAG1 was removed by 3C protease treatment. Then the sample was diluted by the Dilution Buffer HK10 (20 mM HEPES pH 7.5, 10 mM KCl, 5% glycerol, 1 mM DTT, 2 mM MgCl₂) and loaded onto a Mono Q 5/50 GL column (GE Healthcare). Fractions containing pure STAG1 were collected and concentrated. The SA1 sample was supplemented with 20% glycerol (final concentration), flash-frozen in liquid nitrogen, and stored at -80°C.

High Five cells expressing SMC1A, SMC3, and RAD21 with or without NIPBL^C were resuspended in the Lysis Buffer HK150 plus 1 × PierceTM EDTA-free Protease Inhibitor Tablets, 25 U ml⁻¹ PierceTM Universal Nuclease for Cell Lysis, 1 mM PMSF, and 0.04% Tween-20. Cells were lysed by a high-pressure homogenizer, and cleared by centrifugation at 40,000 g for 90 min at 4°C. The supernatant was mixed with 10 ml Amylose Resin (NEB) for 1.5 h at 4°C. The resin was washed with Lysis Buffer HK150 and eluted with Lysis Buffer HK150 plus 20 mM maltose. STAG1 was added to the eluate, incubated on ice for 1 h, and then loaded onto a HiTrap Heparin HP column (GE Healthcare). The fractions containing cohesin or cohesin- NIPBL^C were pooled, diluted with the Dilution Buffer HK10, and then loaded onto a Mono Q 5/50 GL or Resource Q column (GE Healthcare). The complexes were then fractionated on a Superose 6 Increase 10/300 GL column (GE Healthcare) pre-equilibrated in the GF Buffer HK150 (20 mM HEPES pH 7.5, 150 mM KCl, 0.5 mM TCEP and 0.01% IGEPAL® CA-630). The purified complexes were concentrated to 1-4 μM, supplemented with 10% glycerol, flash-frozen in liquid nitrogen, and stored at -80°C.

The ATPase-deficient EQ (SMC1A E1157Q and SMC3 E1144Q) mutant of cohesin was cloned, expressed, and purified as described for the wild-type cohesin. The SNAP_f tag for

fluorescence labeling was inserted into the STAG1 expression plasmid before the TwinStrepII and His dual tag. After ion exchange chromatography, the SNAP-tagged STAG1 protein was incubated with SNAP-Surface Alexa Fluor 647 (New England BioLabs, #S9136S) at a molar ratio of 1:2 at 25°C for 4 h, and then the free dye was removed by gel filtration. Labeled STAG1 was added to cohesin-NIPBL^C without STAG1 and purified as described above.

ATPase assay

The ATPase assay was performed as described in the ADP-Glo™ Kinase Assay manual (Promega). Briefly, 50 nM purified protein complex, 500 nM 40-mer dsDNA (Integrated DNA Technologies, 5'-TTTGAAAAGCAAGCATAAAAGATCTAACATAAAATCTG-3'), and 500 μM ATP in 10 μl ATPase Buffer (20 mM HEPES pH 7.5, 60 mM KCl, 10 mM MgCl₂, 1 mM DTT, 5% glycerol, 0.05% Tween-20) were incubated at 32°C for 20 min. 10 μl ADP-Glo™ Reagent was added and incubated for 40 min. 20 μl Kinase Detection Reagent was added and incubated for 1 h. The luminescence was measured with a VICTOR³V 1420 Multilabel Counter (Perkin Elmer). The data were analyzed with Prism 8 (GraphPad).

Negative stain electron microscopy

The cohesin-NIPBL^C complex was crosslinked with BS³ on ice for 1 h, and then further purified on a Superose 6 Increase 10/300 GL column. For negative staining, the complex was diluted to 10 μg ml⁻¹ in the GF Buffer HK150. 200-mesh copper grids with formvar/carbon film (Electron Microscopy Sciences, #FCF200-Cu) were treated by glow-discharging in the PELCO easiGlow™ Glow Discharge Cleaning System (TedPella). 4 μl sample was applied to the grid and incubated for 30 s. After wash, 4 μl 2% uranyl formate was added to the grid and incubated for 30 s. Data were collected on a 120 kV Tecnai G2 Spirit BioTWIN microscope (FEI) at a magnification of 30,000 ×. Total 40 EM images were collected, and recognizable particles were manually picked and counted.

TIRF microscopy data collection

All single-molecule images were collected with a Nikon Ti-E microscope equipped with a customized prism-TIRF configuration. Experiments were conducted on a floating TMC optical table to avoid spatial drift. Flowcells were illuminated by a 488 nm laser (Coherent) and by a 637 nm laser (Coherent) through a quartz prism (Tower Optical Co.). For imaging YOYO-1-stained DNA for tens of minutes, the laser light was adjusted to deliver low power (~4 mW) at the front face of the prism using a neutral density filter set (Thorlabs). For imaging and photobleaching Alexa647-labeled cohesin, the laser power was adjusted to deliver 20 mW and 110 mW, respectively. Fluorescence was collected by two EM-CCD cameras (Andor iXon DU897, -80°C) using a 638 nm dichroic beam splitter (Chroma). NIS-Elements software (Nikon) was used to collect the single-molecule data at 1-5 s frame rates with 100-250 ms exposure time. All images were saved as TIFF files without compression for further image analysis in FIJI, a distribution of the open-source ImageJ software (NIH) (37).

Preparation of single-molecule DNA substrates

DNA substrates for single-molecule imaging were prepared by modifying the cohesive ends of λ-DNA (NEB). Briefly, 150 μg λ-DNA was mixed with 2 μM YK101 (5Phos-AGGTGGCCGCC-3BioTEG) and YK105 (5Phos-GGGCGGCGACCT) for single-tethered DNA, or YK101 and YK103 (5Phos-GGGCGGCGACCT-3BioTEG) for double-tethered DNA. The mixture was

heated to 70°C for 15 min followed by a gradual cooling to 15°C for 2 h. T4 DNA ligase (NEB) was added to the sample and incubated overnight at room temperature to seal nicks on DNA. The ligase was inactivated with 1.5 M NaCl, and the reaction was passed through an S-1000 (Fisher, 17047601) gel filtration column to remove excess oligonucleotides and proteins. The collected fractions from the first peak normally produced ~12 ml DNA solution and were stored at 4°C.

Nucleosomes were deposited on λ-DNA as described previously (38). Briefly, the DNA was concentrated by isopropanol precipitation and dissolved in 2 M TE buffer (10 mM Tris-HCl pH 8.0, 1 mM EDTA, 2 M NaCl). For reconstitution, 0.8 nM DNA was mixed with human octamers (3xHA-tagged H2A with untagged H2B, H3, H4; Histone Source), and the mixture was dialyzed using a mini dialysis button (10 kDa molecular weight cutoff, BioRad) against 400 ml dialysis buffer (10 mM Tris-HCl pH 7.6, 1 mM EDTA, 1 mM DTT, and gradually decreasing concentrations of NaCl). The ratio of DNA to octamer was adjusted to have 2 to 7 nucleosomes per DNA. For fluorescently labeling nucleosomes, 10 nM anti-HA antibody (Immunology Consultants Laboratory, RHGT-45A-Z) was injected into the flow cell containing nucleosome-bound DNA molecules, and then 10 nM QD705-conjugated secondary antibody (Thermo Fisher) was incubated for 10 min.

Single- and double-tethered DNA assay for single-molecule imaging

Single-tethered DNA molecules were prepared using DNA curtains assembled in custom-made microfluidic chambers. A quartz microscope slide was patterned with 1-2 μm Chromium (Cr) barriers and was passivated with a fluid lipid bilayer (32).

For making U-shaped double-tethered DNA, the surface of the flow cell was initially coated by biotin-BSA followed by streptavidin. For the coating, the biotin-BSA stock solution (10 mg ml⁻¹) was prepared in the T50 buffer (10 mM Tris, 50 mM NaCl, pH 8.0) and stored at 4°C. The solution was diluted 10 times with the T50 buffer right before use and was loaded into the flow cell. After 10-min BSA adsorption, the streptavidin (Thermo Fisher, 434301) solution was loaded into the flow cell (0.1 mg ml⁻¹ in the T50 buffer) and incubated for 10 min at room temperature. For further passivation of the surface to prevent nonspecific adsorption of nucleic acids and proteins, 30 μl of the liposome stock solution (Avanti Polar Lipids; 98 mol% DOPC, 2 mol% DOPE-mPEG2K) was diluted in 800 μl of the lipid buffer (10 mM Tris, 100 mM NaCl, pH 8.0) and loaded into the flow cell. After 20-min incubation, 20 μl of λ-DNA stock was diluted in 1 ml T50 buffer and incubated for 5 min in the chamber. The flow cell was then immediately used for the single-molecule imaging. DNA was stretched and visualized by a continuous flow (0.1 ml min⁻¹) with the imaging buffer (40 mM Tris-HCl pH 8.0, 2 mM MgCl₂, 0.2 mg ml⁻¹ BSA, 50 mM NaCl, 1 mM DTT, and ± 1 mM ATP or AMP-PNP as indicated, 0.2-0.5 nM YOYO-1) supplemented with an oxygen scavenging system (3% D-glucose (w/v), 1 mM Trolox, 1500 units catalase, 250 units glucose oxidase; all from Sigma-Aldrich).

Imaging cohesin-NIPBL^C on DNA

Two different imaging strategies were used to observe cohesin-NIPBL^C on DNA. Quantum dots (QDs) are relatively large (~5-10 nm diameter) but excellent fluors for single-molecule particle tracking (i.e., bright, photostable, and commonly used in single-molecule experiments) (39). Therefore, we fluorescently labeled the N-terminal His₆ of NIPBL^C with an antibody-conjugated QD for long-term imaging. 5 nM of His₆-tagged cohesin-NIPBL^C was incubated with 7 nM anti-His₆ antibody (Takara, 631212) and 10 nM anti-mouse QDs (Thermo Fisher, Q11062MP) in a total volume of 50 μl on ice for 7 min. The mixture was then diluted to a total volume of 150 μl

in the BSA buffer (40 mM Tris-HCl pH 8.0, 2 mM MgCl₂, 0.2 mg ml⁻¹ BSA, 50 mM NaCl, 1 mM DTT, and ± 1 mM nucleotide). To count cohesin complexes via photobleaching, and to avoid potential effects of the large QDs on cohesin motor activity, we also labeled complexes with Alexa647, a small organic fluor. For imaging Alexa647-labeled proteins, 1 μM protein stock was diluted to 1-3 nM in the same BSA buffer. Immediately after the conjugation or dilution, the fluorescently labeled proteins were injected into the flowcell at a 0.1 ml min⁻¹ flow rate. The enzyme activity and loop extrusion rates were very similar between the unlabeled, QD- and Alexa647-labeled complexes (fig. S8B).

Single-molecule data analysis

Fluorescence images were analyzed using ImageJ and MATLAB (Mathworks) scripts. The degree of DNA compaction was assessed by measuring the end-to-end distance of DNA. The rate of condensation was measured by the initial slope during the compaction using ImageJ. For the creation of fluorescence intensity profiles showing looped DNA, seven pixels across the DNA axis were taken in each frame, and background intensity was subtracted. Subsequently, the intensity values from the seven pixels at each row were summed, and each summed value was plotted to build an intensity kymograph. For the detection of DNA loop positions along the DNA axis, the summed values were normalized to a maximum value in each frame to obtain a relative brightness profile, which was used to infer the loop positions.

We estimated the force applied by constant sheer flow by measuring the DNA extension relative to B-form DNA prior to injecting cohesin (fig. S2C). DNA extension can be calibrated via the Worm-Like-Chain (WLC) model. The WLC is suitable for describing the large-scale end-to-end dynamics of polymer chains, including double-stranded DNA molecules under sheer flow (40, 41). The estimated applied forces are thus calculated on single-tethered DNA molecule prior to loop extrusion. In the WLC model, the applied force, F , is:

$$F = \frac{k_B T}{P} \left[\frac{1}{4} \left(1 - \frac{x}{L_0} \right)^{-2} - \frac{1}{4} + \frac{x}{L_0} \right]$$

where k_B is the Boltzmann constant, T is the absolute temperature, P is the persistence length, L_0 is the contour length of λ-DNA, and x is the measured extension of λ-DNA. These biophysical parameters have all been verified experimentally for this exact substrate, so the force can be directly related to the experimentally measured DNA extension (35).

In the single-tethered DNA assay, most cohesins start loop extrusion near the free DNA end. The force that we report is thus only applicable in the first seconds of loop extrusion. For both single-tethered and U-shaped DNA molecules, tension will continue to increase until the cohesin eventually stalls or reaches the surface tether point.

The number of cohesin-NIPBL^C was inferred from the number of Alexa647 by photobleaching experiment. First, we selected DNA-bound Alexa647 foci with a 10x10 pixel bounding box and subtracted background intensity. The photobleaching traces from individual focus were obtained using ImageJ, and the average intensity from single Alexa647 was determined from a Gaussian fit to the histogram of single step intensities. Next, the initial fluorescent intensity of each focus was divided by the average intensity of single Alexa647 to determine the number of Alexa647-proteins.

Diffusion data were analyzed as described previously (38). QD-labeled cohesin-NIPBL^C proteins were tracked in ImageJ with a custom-written particle tracking script. The trajectories were further analyzed in MATLAB to calculate one-dimensional mean squared displacement (MSD) as a function of the time interval (350 ms and 180 ms for with and without ATP conditions, respectively).

Statistical methods

The two-sample t-test was used to determine whether the averages of the distributions differ between experimental conditions using the PAST3 software package (42). Error bars on the binding distribution histogram were calculated in MATLAB using bootstrap analysis with replacement (43). The significance threshold was set at 0.05 in all tests.

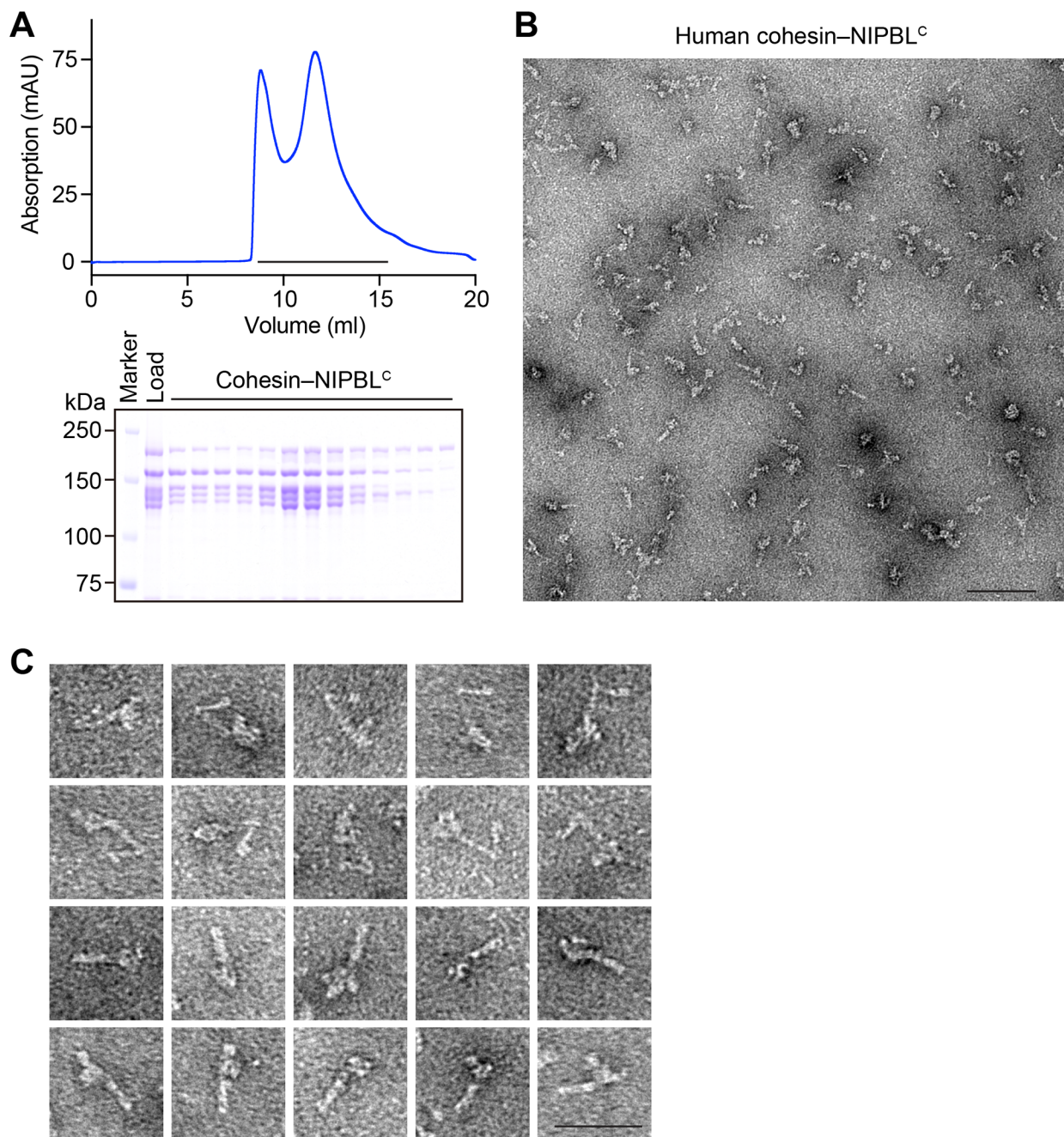


Fig. S1. Characterization of the recombinant human cohesin-NIPBL^C complex. (A) The UV₂₈₀ trace (top panel) and Coomassie stained gel (bottom panel) of the recombinant human cohesin-NIPBL^C complex fractionated on a Superose 6 column. (B) A field of view showing cohesin-NIPBL^C complexes on the EM grid stained with uranyl formate. Scale bar, 100 nm. (C) Representative particles from the negative stain electron micrograph of human cohesin-NIPBL^C complex. Scale bar, 50 nm.

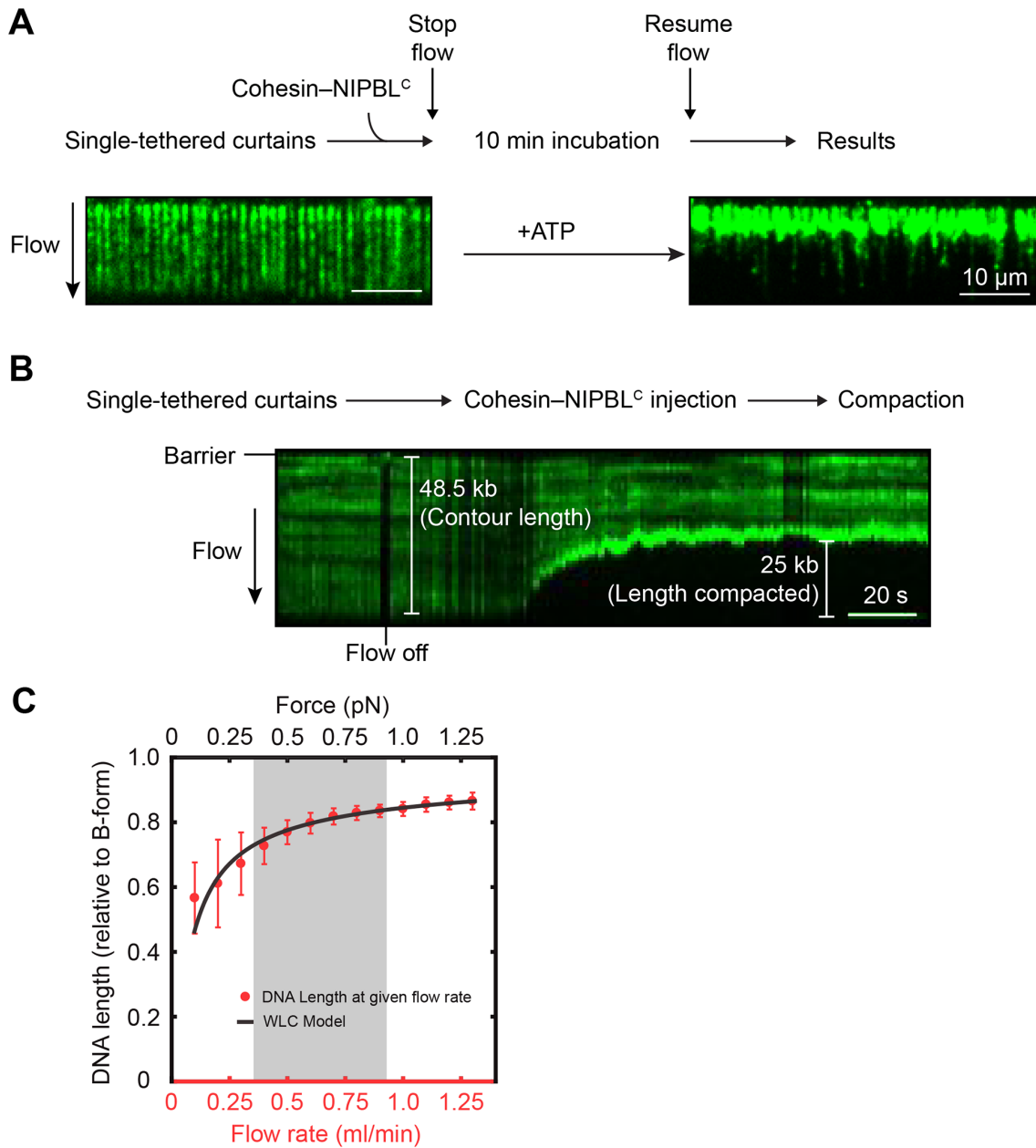


Fig. S2. Visualization of DNA compaction mediated by cohesin–NIPBL^C. (A) Representative images of single-tethered DNA curtains before and after protein incubation. In the presence of ATP, the DNA array was fully compacted to the barrier after a 10-min incubation with the cohesin–NIPBL^C complexes. This compaction was not reversed by resuming the buffer flow. (B) Kymograph showing partial condensation of YOYO-1-stained DNA by cohesin–NIPBL^C. DNA is stretched by a continuous flow of a 25 mM NaCl buffer. (C) Relationship between the applied flow rate and DNA length (mean \pm SD) relative to DNA B-form contour length, fitted to the Worm-Like Chain Model (solid line) with the fitted persistence length of 43 ± 3 nm and a contour length of 16.3 ± 0.1 μ m. Gray square indicates the flow regime used in this study. Adapted from (35).

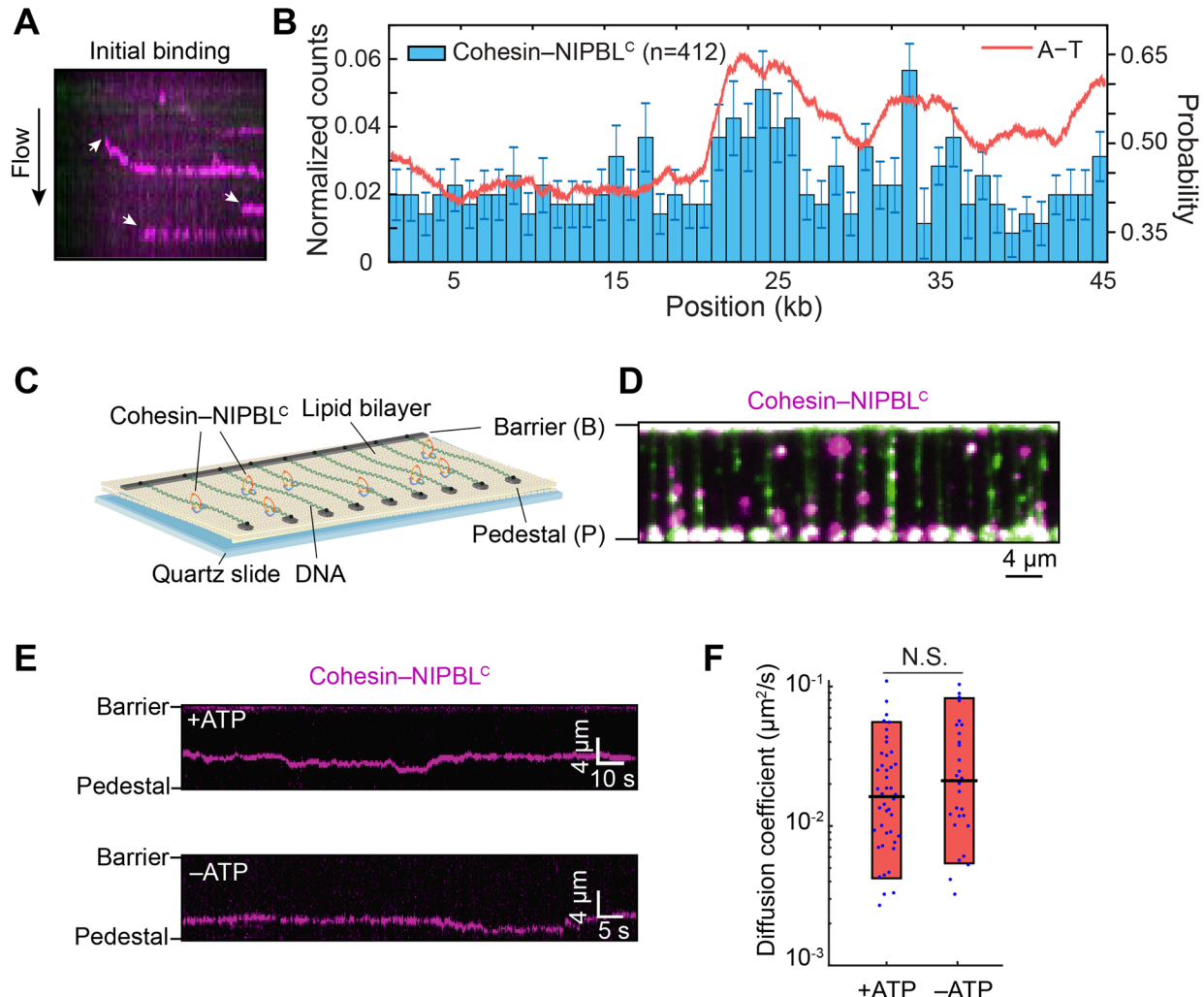


Fig. S3. Binding and diffusion of cohesin-NIPBL^c on DNA. (A) NIPBL^c (magenta) on a single DNA. (B) Histogram showing the initial binding distribution of human cohesin-NIPBL^c bound on the DNA substrate (n=412 cohesin complexes). The A-T content over a corresponding 100-bp window is shown as a red line. (C) Illustration of a double-tethered DNA curtain. Buffer flow is stopped after the DNA is captured between the barriers and pedestals. (D) Image of QD-labeled cohesin-NIPBL^c loaded on double-tethered DNA curtain. (E) Representative kymographs of cohesin-NIPBL^c complexes with and without ATP. (F) Diffusion coefficients of cohesin-NIPBL^c complexes in the presence and absence of ATP. Boxplots indicate the median, 10th, and 90th percentiles of the distribution. N.S., not significant.

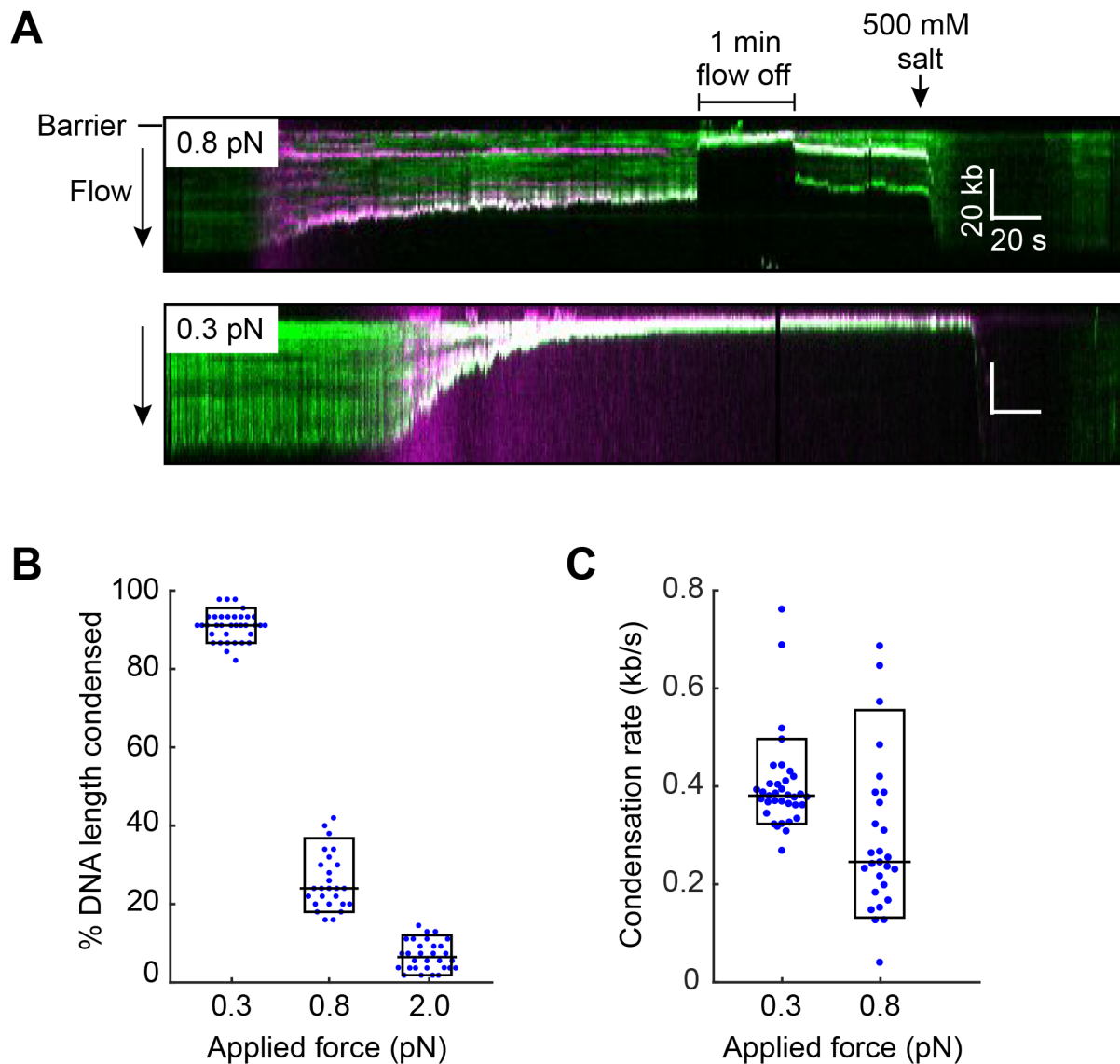


Fig. S4. DNA condensation by cohesin-NIPBL^C in a 25 mM NaCl buffer. (A) Representative kymographs showing gradual DNA condensation under continuous buffer flow that exerts an applied force of approximately 0.8 pN (top) or 0.3 pN (bottom). DNA is completely compacted to the barrier at low force. Injection of a high-salt buffer (500 mM) completely reversed this compaction. (B) Quantification of the percentage of DNA condensed at different forces applied on the single-tethered DNA curtains. (C) Quantification of the rate of DNA compaction at low and high applied forces. The rate could not be measured accurately for an applied force of ~2.0 pN.

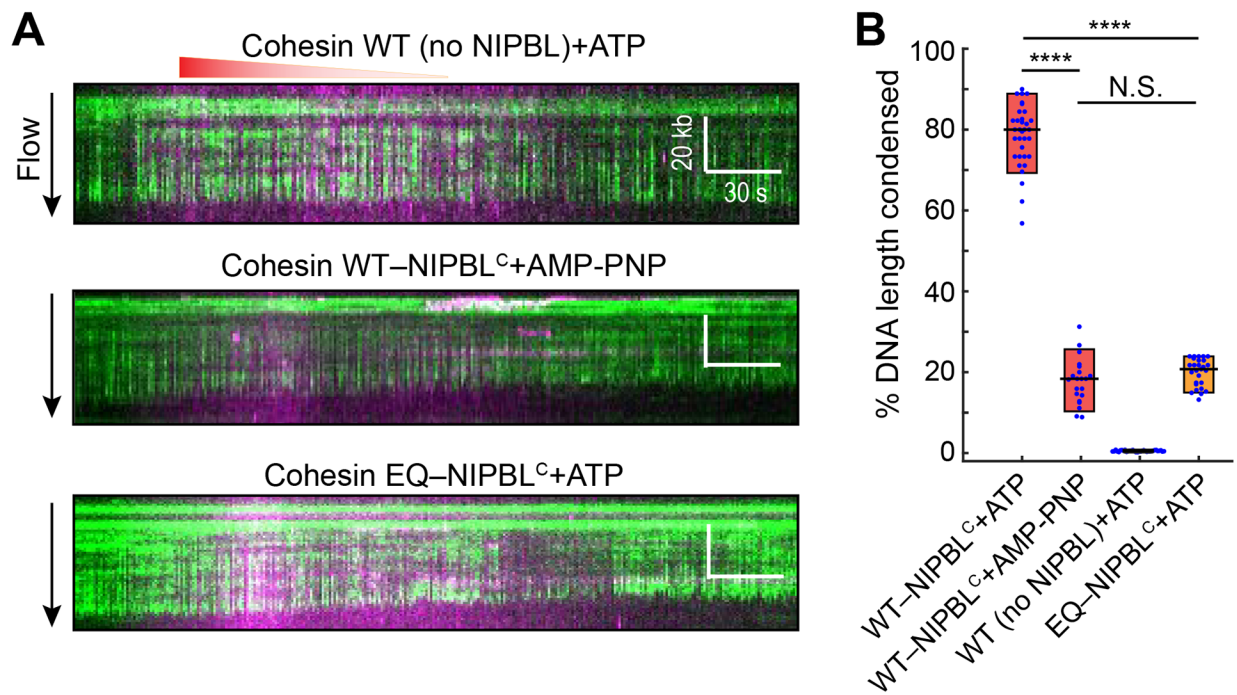


Fig. S5. Cohesin-mediated DNA compaction requires ATP and NIPBL. (A) Representative kymographs of the wild type (WT) cohesin complex alone with ATP, the cohesin WT-NIPBL^c complex with AMP-PNP, and the cohesin EQ-NIPBL^c complex with ATP. (B) Percentage of DNA length condensed for the indicated cohesin WT and EQ complexes with different nucleotides.

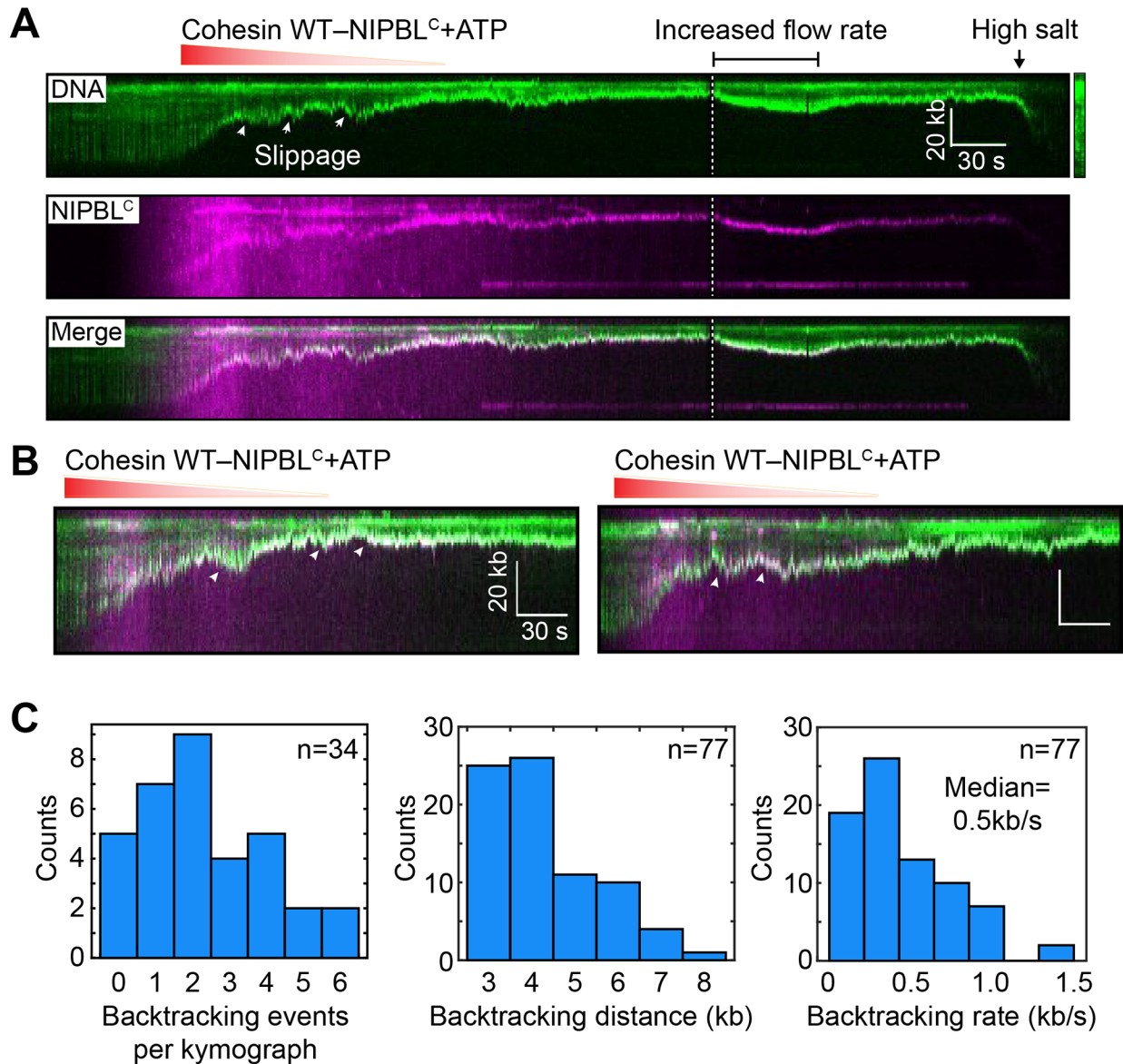


Fig. S6. Cohesin-NIPBL^C backtracks during DNA compaction. (A) Representative kymograph showing the condensation of single-tethered DNA (top panel) by QD-tagged cohesin-NIPBL^C (middle panel). Overlay of the DNA and QD channels (bottom panel) shows that the protein complex tracks the end of the DNA undergoing condensation. The intermittent slippage events are indicated by white arrows. The white dashed line marks the timepoint when the applied force is increased from low (~0.3 pN) to high (~0.8 pN) for a 1-min duration. The black arrow indicates the injection of high salt (500 mM NaCl) buffer. Because the high-salt buffer washes away YOYO-1 and dims the fluorescence of DNA, a contrast-adjusted DNA image is shown to the right of the DNA kymograph for better visualization of the extended DNA. (B) Additional representative kymographs showing transient slippage events at 50 mM NaCl. (C) Quantification of cohesin backtracking events.

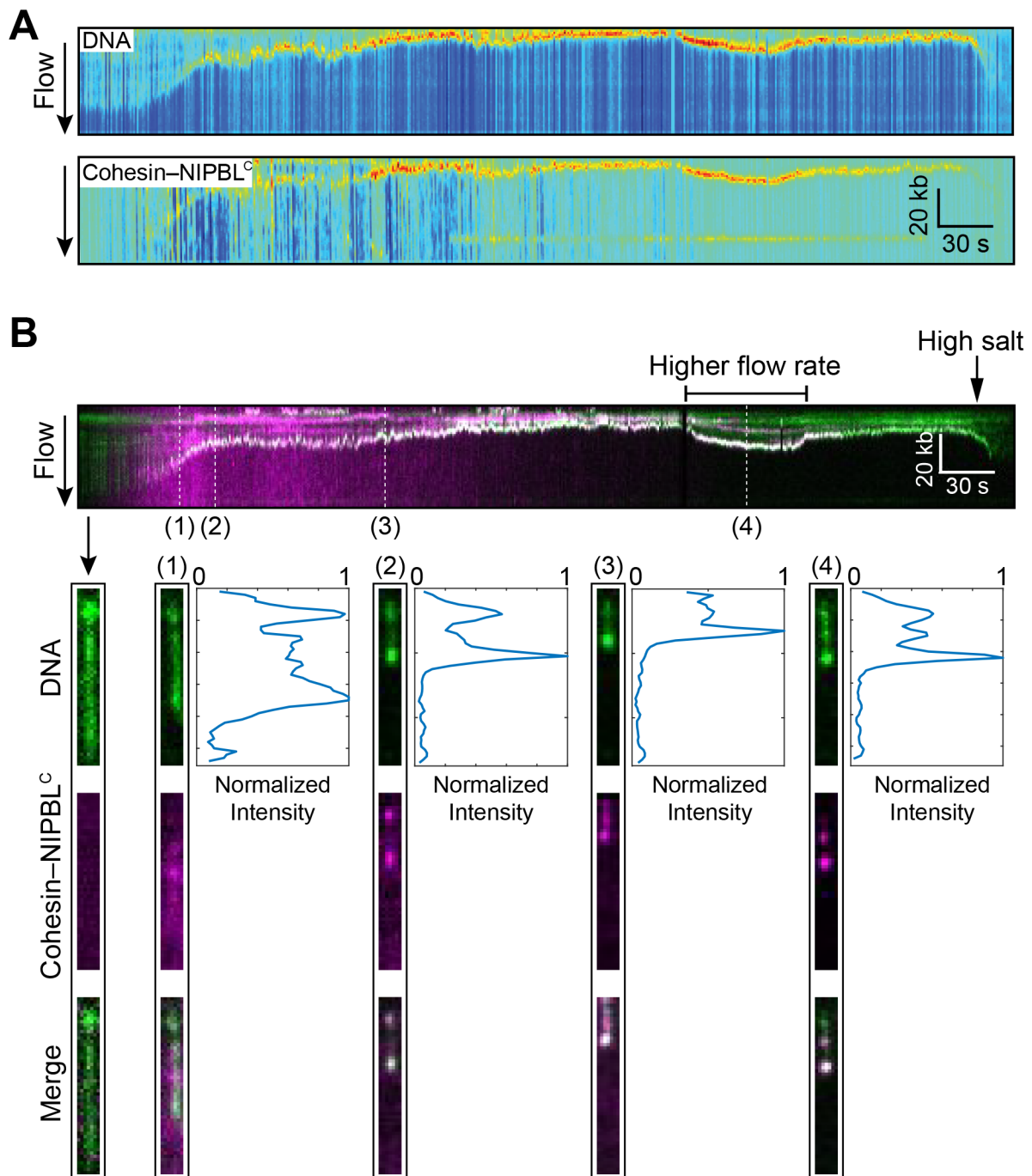


Fig. S7. DNA compaction by cohesin–NIPBL^C preferentially starts at the end of DNA. (A) Kymograph showing the fluorescent intensity profiles of the DNA and protein molecules described in fig. S6A. (B) Kymograph and a montage of images at the indicated timepoints showing separate and merged channels of DNA and protein. Relative fluorescent intensities of YOYO-1-stained DNA is shown to the right of the compacting DNA.

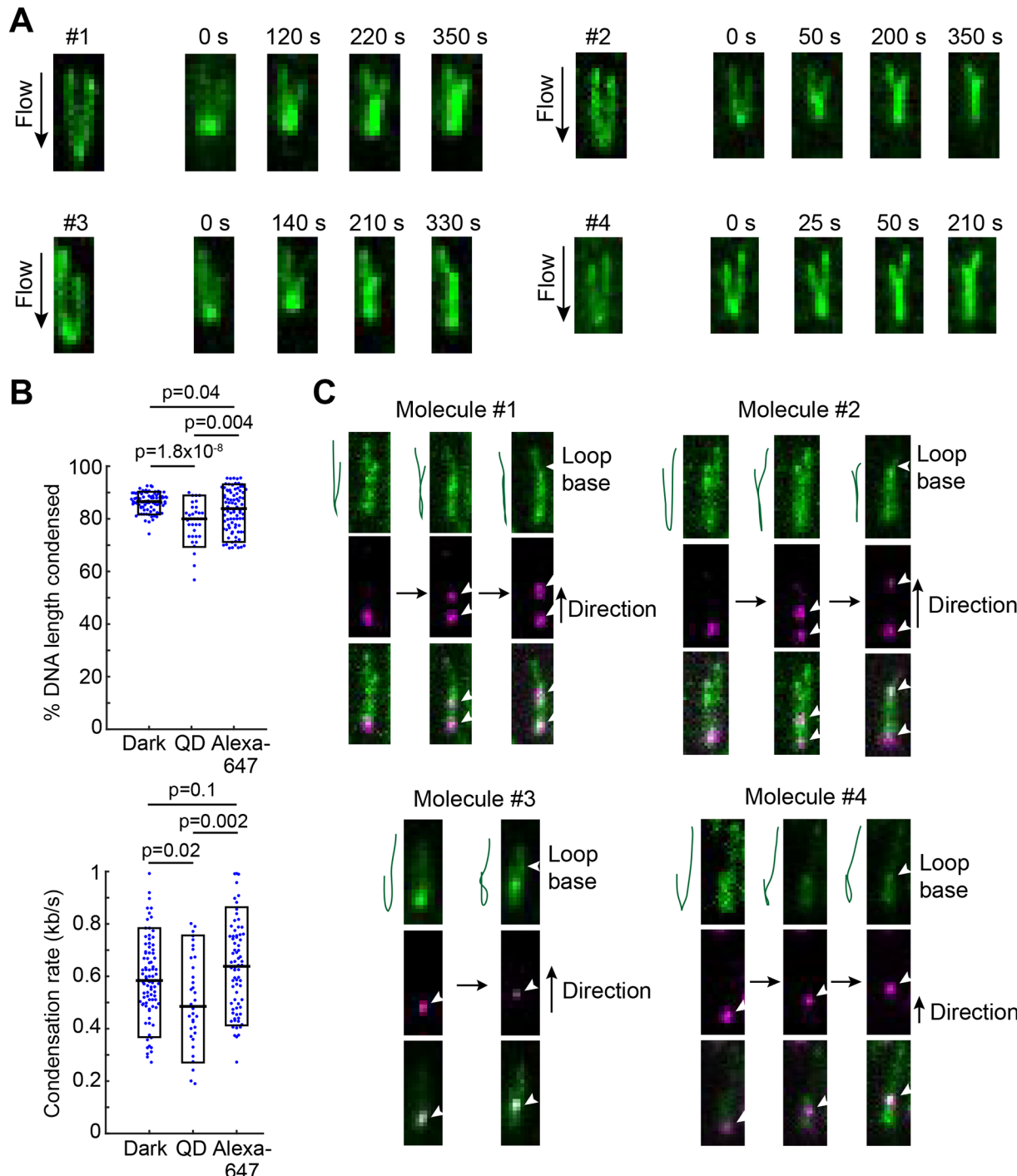


Fig. S8. DNA loop extrusion by cohesin-NIPBL^C. (A) Time-course montages showing four examples of DNA loop extrusion by cohesin-NIPBL^C on YOYO-1 stained 'U'-shaped DNA. (B) Comparison of unlabeled and fluorescent (QD or Alexa647) cohesin-NIPBL^C motor activities on YOYO-1 stained DNA. (B) Time-course montages showing four examples of cohesin-NIPBL^C localization at the DNA loop base. Arrowheads indicate the labeled cohesin-NIPBL^C and the base of the loop.

Supplementary Movies Legends

Movie S1. A single-tethered DNA curtain that is homogeneously stained with YOYO-1 and stretched by flow at 0.1 ml min^{-1} .

Movie S2. Compaction of single-tethered DNA by cohesin-NIPBL^C.

Movie S3. Injection of a high-salt buffer fully reverses cohesin-NIPBL^C-mediated DNA compaction.

Movie S4. YOYO-1 stained ‘U’-shaped DNA has a homogeneous intensity profile in the absence of cohesin-NIPBL^C.

Movies S5, S6, S7. Loop extrusion of YOYO-1 stained DNA under a constant flow by cohesin-NIPBL^C.

Movie S8. Rapid DNA loop disruption during a high-salt wash.

Movie S9. Alexa647-labeled cohesin-NIPBL^C (magenta) localizes at the base of a DNA loop (green).

References and Notes

1. J. H. Haarhuis, A. M. Elbatsh, B. D. Rowland, Cohesin and its regulation: On the logic of X-shaped chromosomes. *Dev. Cell* **31**, 7–18 (2014). [doi:10.1016/j.devcel.2014.09.010](https://doi.org/10.1016/j.devcel.2014.09.010) [Medline](#)
2. C. Morales, A. Losada, Establishing and dissolving cohesion during the vertebrate cell cycle. *Curr. Opin. Cell Biol.* **52**, 51–57 (2018). [doi:10.1016/j.ceb.2018.01.010](https://doi.org/10.1016/j.ceb.2018.01.010) [Medline](#)
3. F. Uhlmann, SMC complexes: From DNA to chromosomes. *Nat. Rev. Mol. Cell Biol.* **17**, 399–412 (2016). [doi:10.1038/nrm.2016.30](https://doi.org/10.1038/nrm.2016.30) [Medline](#)
4. G. Zheng, H. Yu, Regulation of sister chromatid cohesion during the mitotic cell cycle. *Sci. China Life Sci.* **58**, 1089–1098 (2015). [doi:10.1007/s11427-015-4956-7](https://doi.org/10.1007/s11427-015-4956-7) [Medline](#)
5. Á. Sedeño Cacciatore, B. D. Rowland, Loop formation by SMC complexes: Turning heads, bending elbows, and fixed anchors. *Curr. Opin. Genet. Dev.* **55**, 11–18 (2019). [doi:10.1016/j.gde.2019.04.010](https://doi.org/10.1016/j.gde.2019.04.010) [Medline](#)
6. J. M. Peters, A. Tedeschi, J. Schmitz, The cohesin complex and its roles in chromosome biology. *Genes Dev.* **22**, 3089–3114 (2008). [doi:10.1101/gad.1724308](https://doi.org/10.1101/gad.1724308) [Medline](#)
7. K. Nasmyth, C. H. Haering, Cohesin: Its roles and mechanisms. *Annu. Rev. Genet.* **43**, 525–558 (2009). [doi:10.1146/annurev-genet-102108-134233](https://doi.org/10.1146/annurev-genet-102108-134233) [Medline](#)
8. R. Ciosk, M. Shirayama, A. Shevchenko, T. Tanaka, A. Toth, A. Shevchenko, K. Nasmyth, Cohesin’s binding to chromosomes depends on a separate complex consisting of Scc2 and Scc4 proteins. *Mol. Cell* **5**, 243–254 (2000). [doi:10.1016/S1097-2765\(00\)80420-7](https://doi.org/10.1016/S1097-2765(00)80420-7) [Medline](#)
9. E. T. Tonkin, T. J. Wang, S. Lisgo, M. J. Bamshad, T. Strachan, NIPBL, encoding a homolog of fungal Scc2-type sister chromatid cohesion proteins and fly Nipped-B, is mutated in Cornelia de Lange syndrome. *Nat. Genet.* **36**, 636–641 (2004). [doi:10.1038/ng1363](https://doi.org/10.1038/ng1363) [Medline](#)
10. E. Watrin, A. Schleiffer, K. Tanaka, F. Eisenhaber, K. Nasmyth, J.-M. Peters, Human Scc4 is required for cohesin binding to chromatin, sister-chromatid cohesion, and mitotic progression. *Curr. Biol.* **16**, 863–874 (2006). [doi:10.1016/j.cub.2006.03.049](https://doi.org/10.1016/j.cub.2006.03.049) [Medline](#)
11. T. Bose, J. L. Gerton, Cohesinopathies, gene expression, and chromatin organization. *J. Cell Biol.* **189**, 201–210 (2010). [doi:10.1083/jcb.200912129](https://doi.org/10.1083/jcb.200912129) [Medline](#)
12. K. Nasmyth, Disseminating the genome: Joining, resolving, and separating sister chromatids during mitosis and meiosis. *Annu. Rev. Genet.* **35**, 673–745 (2001). [doi:10.1146/annurev.genet.35.102401.091334](https://doi.org/10.1146/annurev.genet.35.102401.091334) [Medline](#)
13. E. Alipour, J. F. Marko, Self-organization of domain structures by DNA-loop-extruding enzymes. *Nucleic Acids Res.* **40**, 11202–11212 (2012). [doi:10.1093/nar/gks925](https://doi.org/10.1093/nar/gks925) [Medline](#)
14. J. Gassler, H. B. Brandão, M. Imakaev, I. M. Flyamer, S. Ladstätter, W. A. Bickmore, J.-M. Peters, L. A. Mirny, K. Tachibana, A mechanism of cohesin-dependent loop extrusion organizes zygotic genome architecture. *EMBO J.* **36**, 3600–3618 (2017). [doi:10.15252/embj.201798083](https://doi.org/10.15252/embj.201798083) [Medline](#)

15. J. H. I. Haarhuis, R. H. van der Weide, V. A. Blomen, J. O. Yáñez-Cuna, M. Amendola, M. S. van Ruiten, P. H. L. Krijger, H. Teunissen, R. H. Medema, B. van Steensel, T. R. Brummelkamp, E. de Wit, B. D. Rowland, The cohesin release factor WAPL restricts chromatin loop extension. *Cell* **169**, 693–707.e14 (2017). [doi:10.1016/j.cell.2017.04.013](https://doi.org/10.1016/j.cell.2017.04.013) [Medline](#)
16. S. S. P. Rao, S.-C. Huang, B. Glenn St Hilaire, J. M. Engreitz, E. M. Perez, K.-R. Kieffer-Kwon, A. L. Sanborn, S. E. Johnstone, G. D. Bascom, I. D. Bochkov, X. Huang, M. S. Shamim, J. Shin, D. Turner, Z. Ye, A. D. Omer, J. T. Robinson, T. Schlick, B. E. Bernstein, R. Casellas, E. S. Lander, E. L. Aiden, Cohesin loss eliminates all loop domains. *Cell* **171**, 305–320.e24 (2017). [doi:10.1016/j.cell.2017.09.026](https://doi.org/10.1016/j.cell.2017.09.026) [Medline](#)
17. G. Wutz, C. Várnai, K. Nagasaka, D. A. Cisneros, R. R. Stocsits, W. Tang, S. Schoenfelder, G. Jessberger, M. Muhar, M. J. Hossain, N. Walther, B. Koch, M. Kueblbeck, J. Ellenberg, J. Zuber, P. Fraser, J.-M. Peters, Topologically associating domains and chromatin loops depend on cohesin and are regulated by CTCF, WAPL, and PDS5 proteins. *EMBO J.* **36**, 3573–3599 (2017). [doi:10.15252/embj.201798004](https://doi.org/10.15252/embj.201798004) [Medline](#)
18. L. Vian, A. Pękowska, S. S. P. Rao, K.-R. Kieffer-Kwon, S. Jung, L. Baranello, S.-C. Huang, L. El Khattabi, M. Dose, N. Pruett, A. L. Sanborn, A. Canela, Y. Maman, A. Oksanen, W. Resch, X. Li, B. Lee, A. L. Kovalchuk, Z. Tang, S. Nelson, M. Di Pierro, R. R. Cheng, I. Machol, B. G. St Hilaire, N. C. Durand, M. S. Shamim, E. K. Stamenova, J. N. Onuchic, Y. Ruan, A. Nussenzweig, D. Levens, E. L. Aiden, R. Casellas, The energetics and physiological impact of cohesin extrusion. *Cell* **173**, 1165–1178.e20 (2018). [doi:10.1016/j.cell.2018.03.072](https://doi.org/10.1016/j.cell.2018.03.072) [Medline](#)
19. G. Fudenberg, M. Imakaev, C. Lu, A. Goloborodko, N. Abdennur, L. A. Mirny, Formation of chromosomal domains by loop extrusion. *Cell Rep.* **15**, 2038–2049 (2016). [doi:10.1016/j.celrep.2016.04.085](https://doi.org/10.1016/j.celrep.2016.04.085) [Medline](#)
20. A. Tedeschi, G. Wutz, S. Huet, M. Jaritz, A. Wuensche, E. Schirghuber, I. F. Davidson, W. Tang, D. A. Cisneros, V. Bhaskara, T. Nishiyama, A. Vaziri, A. Wutz, J. Ellenberg, J.-M. Peters, Wapl is an essential regulator of chromatin structure and chromosome segregation. *Nature* **501**, 564–568 (2013). [doi:10.1038/nature12471](https://doi.org/10.1038/nature12471) [Medline](#)
21. T. Terakawa, S. Bisht, J. M. Eeftens, C. Dekker, C. H. Haering, E. C. Greene, The condensin complex is a mechanochemical motor that translocates along DNA. *Science* **358**, 672–676 (2017). [doi:10.1126/science.aan6516](https://doi.org/10.1126/science.aan6516) [Medline](#)
22. M. Ganji, I. A. Shaltiel, S. Bisht, E. Kim, A. Kalichava, C. H. Haering, C. Dekker, Real-time imaging of DNA loop extrusion by condensin. *Science* **360**, 102–105 (2018). [doi:10.1126/science.aar7831](https://doi.org/10.1126/science.aar7831) [Medline](#)
23. I. F. Davidson, D. Goetz, M. P. Zaczek, M. I. Molodtsov, P. J. Huis In 't Veld, F. Weissmann, G. Litos, D. A. Cisneros, M. Ocampo-Hafalla, R. Ladurner, F. Uhlmann, A. Vaziri, J.-M. Peters, Rapid movement and transcriptional re-localization of human cohesin on DNA. *EMBO J.* **35**, 2671–2685 (2016). [doi:10.15252/embj.201695402](https://doi.org/10.15252/embj.201695402) [Medline](#)
24. J. Stigler, G. O. Çamdere, D. E. Koshland, E. C. Greene, Single-molecule imaging reveals a collapsed conformational state for DNA-bound cohesin. *Cell Rep.* **15**, 988–998 (2016). [doi:10.1016/j.celrep.2016.04.003](https://doi.org/10.1016/j.celrep.2016.04.003) [Medline](#)

25. M. Kanke, E. Tahara, P. J. Huis In't Veld, T. Nishiyama, Cohesin acetylation and Wapl-Pds5 oppositely regulate translocation of cohesin along DNA. *EMBO J.* **35**, 2686–2698 (2016). [doi:10.15252/embj.201695756](https://doi.org/10.15252/embj.201695756) [Medline](#)
26. J. Rhodes, D. Mazza, K. Nasmyth, S. Uphoff, Scc2/Nipbl hops between chromosomal cohesin rings after loading. *eLife* **6**, e30000 (2017). [doi:10.7554/eLife.30000](https://doi.org/10.7554/eLife.30000) [Medline](#)
27. G. Zheng, M. Kanchwala, C. Xing, H. Yu, MCM2-7-dependent cohesin loading during S phase promotes sister-chromatid cohesion. *eLife* **7**, e33920 (2018). [doi:10.7554/eLife.33920](https://doi.org/10.7554/eLife.33920) [Medline](#)
28. N. J. Petela, T. G. Gligoris, J. Metson, B.-G. Lee, M. Voulgaris, B. Hu, S. Kikuchi, C. Chapard, W. Chen, E. Rajendra, M. Srinivasan, H. Yu, J. Löwe, K. A. Nasmyth, Scc2 is a potent activator of cohesin's ATPase that promotes loading by binding Scc1 without Pds5. *Mol. Cell* **70**, 1134–1148.e7 (2018). [doi:10.1016/j.molcel.2018.05.022](https://doi.org/10.1016/j.molcel.2018.05.022) [Medline](#)
29. Y. Murayama, F. Uhlmann, Biochemical reconstitution of topological DNA binding by the cohesin ring. *Nature* **505**, 367–371 (2014). [doi:10.1038/nature12867](https://doi.org/10.1038/nature12867) [Medline](#)
30. M. T. Hons, P. J. Huis In 't Veld, J. Kaesler, P. Rombaut, A. Schleiffer, F. Herzog, H. Stark, J.-M. Peters, Topology and structure of an engineered human cohesin complex bound to Pds5B. *Nat. Commun.* **7**, 12523 (2016). [doi:10.1038/ncomms12523](https://doi.org/10.1038/ncomms12523) [Medline](#)
31. F. Bürmann, B.-G. Lee, T. Than, L. Sinn, F. J. O'Reilly, S. Yatskevich, J. Rappaport, B. Hu, K. Nasmyth, J. Löwe, A folded conformation of MukBEF and cohesin. *Nat. Struct. Mol. Biol.* **26**, 227–236 (2019). [doi:10.1038/s41594-019-0196-z](https://doi.org/10.1038/s41594-019-0196-z) [Medline](#)
32. I. F. Gallardo, P. Pasupathy, M. Brown, C. M. Manhart, D. P. Neikirk, E. Alani, I. J. Finkelstein, High-throughput universal DNA curtain arrays for single-molecule fluorescence imaging. *Langmuir* **31**, 10310–10317 (2015). [doi:10.1021/acs.langmuir.5b02416](https://doi.org/10.1021/acs.langmuir.5b02416) [Medline](#)
33. M. M. Soniat, L. R. Myler, J. M. Schaub, Y. Kim, I. F. Gallardo, I. J. Finkelstein, Next-generation DNA curtains for single-molecule studies of homologous recombination. *Methods Enzymol.* **592**, 259–281 (2017). [doi:10.1016/bs.mie.2017.03.011](https://doi.org/10.1016/bs.mie.2017.03.011) [Medline](#)
34. M. Kuno, D. P. Fromm, H. F. Hamann, A. Gallagher, D. J. Nesbitt, Nonexponential “blinking” kinetics of single CdSe quantum dots: A universal power law behavior. *J. Chem. Phys.* **112**, 3117–3120 (2000). [doi:10.1063/1.480896](https://doi.org/10.1063/1.480896)
35. J. M. Schaub, H. Zhang, M. M. Soniat, I. J. Finkelstein, Assessing protein dynamics on low-complexity single-stranded DNA curtains. *Langmuir* **34**, 14882–14890 (2018). [doi:10.1021/acs.langmuir.8b01812](https://doi.org/10.1021/acs.langmuir.8b01812) [Medline](#)
36. F. Weissmann, G. Petzold, R. VanderLinden, P. J. Huis In 't Veld, N. G. Brown, F. Lampert, S. Westermann, H. Stark, B. A. Schulman, J.-M. Peters, biGBac enables rapid gene assembly for the expression of large multisubunit protein complexes. *Proc. Natl. Acad. Sci. U.S.A.* **113**, E2564–E2569 (2016). [doi:10.1073/pnas.1604935113](https://doi.org/10.1073/pnas.1604935113) [Medline](#)
37. J. Schindelin, I. Arganda-Carreras, E. Frise, V. Kaynig, M. Longair, T. Pietzsch, S. Preibisch, C. Rueden, S. Saalfeld, B. Schmid, J.-Y. Tinevez, D. J. White, V. Hartenstein, K. Eliceiri, P. Tomancak, A. Cardona, Fiji: An open-source platform for biological-image analysis. *Nat. Methods* **9**, 676–682 (2012). [doi:10.1038/nmeth.2019](https://doi.org/10.1038/nmeth.2019) [Medline](#)

38. Y. Kim, C. M. Furman, C. M. Manhart, E. Alani, I. J. Finkelstein, Intrinsically disordered regions regulate both catalytic and non-catalytic activities of the MutL α mismatch repair complex. *Nucleic Acids Res.* **47**, 1823–1835 (2019). [Medline](#)
39. K. D. Wegner, N. Hildebrandt, Quantum dots: Bright and versatile in vitro and in vivo fluorescence imaging biosensors. *Chem. Soc. Rev.* **44**, 4792–4834 (2015).
[doi:10.1039/C4CS00532E](https://doi.org/10.1039/C4CS00532E) [Medline](#)
40. T. T. Perkins, D. E. Smith, R. G. Larson, S. Chu, Stretching of a single tethered polymer in a uniform flow. *Science* **268**, 83–87 (1995). [doi:10.1126/science.7701345](https://doi.org/10.1126/science.7701345) [Medline](#)
41. J. F. Marko, E. D. Siggia, Stretching DNA. *Macromolecules* **28**, 8759–8770 (1995).
[doi:10.1021/ma00130a008](https://doi.org/10.1021/ma00130a008)
42. O. Hammer, D. A. Harper, P. D. Ryan, PAST: Paleontological statistics software package for education and data analysis. *Palaeontol. Electronica* **4**, 1–9 (2001).
43. B. Efron, R. J. Tibshirani, *An Introduction to the Bootstrap* (Chapman & Hall/CRC Monographs on Statistics and Applied Probability 57, CRC, ed. 1, 1994).